3D Modeling of an Inca Site with Fine-scale Terrestrial LiDAR

Boleslo E. Romero

ABSTRACT: There is great potential for superior detailed terrain models using terrestrial LiDAR data. Terrestrial LiDAR is a ground-based, active remote sensing system that emits pulses of light, illuminating locations in the environment and measuring the time it takes for reflected light to return to a sensor. From the duration of the light pulse's time-of-flight, a distance can be calculated. By quickly turning slight angles between measurements, such systems are able to record thousands of distance measurements within a few minutes creating a point cloud from a single region-of-interest scan. Aligning multiple scans together produces detailed three-dimensional (3D) models of complex features with sub-centimeter resolution and high accuracy.

Potential applications in geography are related to investigations of caves, understory biomass, and detailed features in urban settings. The application described here involves the documentation and analysis of water-flow at an early 16th century Inca archaeological site in northern highland Ecuador.

The paper presents the process of developing a 3D model from terrestrial LiDAR scans. Using 3D point cloud data to create a surface representation, several workflow stages are discussed. Topics include implications of point selection, scan alignment, and surface generation operations. Particular attention is paid to the accurate spatial orientation and fine scale required for the analysis of Inca water canals, fountains, and pools.

Aiming to represent complex features with sub-centimeter accuracy, the point data was processed using several different operations, each of which affects the resulting surface quality. To align scans, point clouds were initially transformed into interim surfaces using specific interpolation sampling distances. Unnecessary data were deleted and special care was taken to select appropriate data for manual and statistical 'best-fit' alignment. Once scans were aligned, orientation to survey points was necessary for understanding water-flow. Data reduction of overlapping scan points improved the efficiency of the local neighborhood evaluation in the final surface generation step.

KEYWORDS: Terrestrial LiDAR, 3D, archaeology, terrain, surface modeling

Introduction

Terrestrial LiDAR for coupled human and natural environment studies

Terrestrial LiDAR provides spatial data for surface modeling. The laser scans are quick, allowing for thousands of precise locational measurements within minutes. With abundant data easily collected, detailed surface models are feasible. Such fine-scale representation of surfaces offers opportunities for improved understanding of both the landscape and cultural features.

Physical characteristics of the environment represent the blending of both natural processes and human activities. People alter the environment for purposes of survival and comfort. They seek out essential natural resources and commit significant effort to improving access to these. In doing so, they modify the natural environment, supplying their societies with the means to survive and flourish.

One of the most essential of natural resources is water. It is necessary for the sustenance of life; it enhances human health by flushing pollutants; and it provides comfort in its flow, collection, and overall ambiance. Some societies express their excellence and strength by constructing structures for collecting, containing, and prominently displaying this particularly important and life-giving element (Lansing, 2006; Sherbondy, 1987; Strang, 2004).

The Archaeological Site of Inca-Caranqui

The Inca were especially skilled at channeling water from mountainous sources to their population centers (Wright and Valencia 2000; Wright, 2006). Their empire and laborers were very capable of building structures for obtaining water for sustenance, utility, luxury, expression of control, and ceremonial purposes (Bray 2012). Evidence of their expertise in this arena has endured until the present (Bray and Echeverría 2009).

The archaeological site of Inca-Caranqui in northern highland Ecuador contains a variety of structures, including building foundations, walls, terraces, and water-related features such as canals and the large semi-subterranean water temple that have numerous architectural details of interest. The site is located within a continuously populated place that has been inhabited over the past two millennia by several distinct cultures (Bray and Echeverria 2010). Though Inca-Caranqui has changed since its construction, it exhibits signature Inca stonework throughout the core area of the site. A portion of the site's semi-subterranean temple is shown in Figure 1.

Figure 1: Terrestrial LiDAR scanning at the Inca-Caranqui archaeological site in Ecuador.

Relatively few studies have been undertaken that focus on the Inca's manipulation of water, and none have benefitted from the use of terrestrial LiDAR data. Previous analyses of the Inca's water-flow and collection structures have relied on visual observation, conventional surveys of point locations, and estimates of areas and volumes from rough and sparsely sampled measurements (see, for instance, Wright and Valencia 2000; Wright, 2006). With LiDAR data, detailed and comprehensive surface modeling can better represent the structures of interest.

Features of interest for water-flow analysis surface modeling

Though the ultimate intent of this research is to model surfaces within the site, the water features at the site are the focus of this paper. There are two different types of water canals encountered at the site: grooved or carved stone channels and stone-lined and sometimes capped channels. Some of these canals link to fountain features from which water could flow or spurt. There is also what has been interpreted as a sediment tank and a large, walk-in pool that has been interpreted as a water temple (Bray, 2012) with feeder canals and drains that could have been used for either small flows or large collections of water.

With respect to the present surface modeling analysis, the results of creating a fine-scale representation of canal and fountain details should be sufficient for future modeling of larger features like the tank, pool, and temple. Example features of interest are shown in Figure 2. Examples of results throughout the paper follow this image order.

Figure 2: Examples of carved stone canal spouts, covered and uncovered stone-lined canals, and a carved stone fountain situated within a stairwell of the semi-subterranean temple.

The specific aim of this investigation is to evaluate methods of creating detailed surface representations of Inca structures associated with water-flow and collection. Compared to conventional survey and estimation techniques, using terrestrial LiDAR data to model

visible surfaces is expected to provide a more complete and nuanced representation of the Inca's landscape modifications. Improving the surface modeling process will enhance future water-flow analyses at the site.

The process evaluated in this paper involved a commercial software package from InnovMetric named Polyworks (version 11) (InnovMetric, 2012). It is used for creating three-dimensional (3D) polygonal models from point clouds that are composed of multiple individual LiDAR scans.

Scans were first imported and converted to an *interpolated grid image*. The images were then aligned and data points were reduced in overlapping areas. Finally, 3D polygonal models were created for representing the archaeological features. Parameters at various stages greatly affected the characteristics of the resulting surface model. Acceptable parameters were selected through visual analysis and comparison to photographs and site measurements. The specific aim of parameter selections in this case was to identify those that produced a detailed 3D surface model for a comprehensive water-flow analysis at this Inca site.

3D surface modeling description

Data collection

Topographic data collection was performed at Inca Caranqui over three field seasons from 2008-2012 producing terrestrial LiDAR and conventional survey data as listed in Table 1. For this paper, portions of the 2008 LiDAR scans and the 2010 survey points were used.

Table 1: Topographic data collected.

Year	*Terrestrial LiDAR Scanning*	*Conventional Survey*
2008	XYZ and Intensity: Site (40 low-resolution scans) Features (43 high-resolution scans)	
2009	XYZ, Intensity, and RGB color: Features (90 very-high-resolution scans)	1132 points for horizontal and vertical control and feature locations.
2010		1155 points for horizontal and vertical control and feature locations.

An Optech 36D laser scanner was used for terrestrial LiDAR data collection and a Leica TPS Series TC400 total station was used for collecting conventional survey points. Three site benchmarks were used as control points for both types of data. Regarding the LiDAR scans, the entire site of approximately 115 by 45 meters (m) was first scanned at a low resolution, to establish the spatial configuration of features. Then, higher resolutions were

used for particular features of interest, including but not limited to: the semi-subterranean temple, the tank, several canals, fountains, and drains. Since the scanner collects data radially from a point, resolution is generally higher near the scanner. The step-angle resolution at a particular distance can be specified. For the 2008 data discussed in this paper, low-resolution site scans were generally set to have a precision of 50.3 millimeters (mm) at 40 m distance. For features of interest, such as the main 10 by 16 m pool in the temple, high-resolution scans were generally set to have a precision of 14.9 mm at 40 m distance.

The terrestrial LiDAR data is expected to provide a detailed and relatively continuous model of visible surfaces at the site. For example, instead of collecting just a few sample locations from the temple boundary and interior, millions of LiDAR samples were collected. Rough dimensions of the temple could be estimated from conventional survey points, but here, nuanced construction such as subtle flow lines draining canals and floors may be revealed with the LiDAR data. Similarly, the meandering canals may be better represented with numerous samples every few millimeters.

Importing scans

Importing the LiDAR scans into the Polyworks IMAlign module converts the raw data to an *interpolated grid image*. Though there are several settings for managing the interpolation, three main parameters are of interest here. The *maximum angle* restricts the selection of points included in the grid, based upon the angle between the normal vector of the interpolated grid and the direction of the scanner. The *interpolation step* specifies the distance between grid sampling points. The *maximum edge length* defines the maximum length of triangle edges connecting scan points. The *interpolated grid* parameters are critical to the alignment and surface generation processes. The three following sections describe these parameters and their implications along with specific selections for this application. The import parameter settings for the example figures are listed in Table 2 and the examples of each set of results will follow this configuration.

Table 2: Merging parameter settings for examples.

Maximum Angle	*Maximum Edge Length*	*Interpolation Step*
89	0.06	0.01
85	0.06	0.01
80	0.06	0.01
85	**0.06**	0.01
85	**0.04**	0.01
85	**0.02**	0.01
85	0.06	**0.01**
85	0.06	**0.008**
85	0.06	**0.005**

Import parameter: Maximum angle

The *maximum angle* point selection parameter greatly alleviates an issue with some terrestrial LiDAR data. From the duration of the light pulse's time-of-flight, a distance is estimated between the scanner and a surface. Since the beam of light and the sensor are not dimensionless, a small surface area reflects the light and a small sensor area detects the light. There is usually not much noise with the time-measurement when the surface normal is parallel to the light beam (i.e. when the surface is perpendicular to the scanner).

On the other hand, when the surface normal is nearly perpendicular to the light beam (and the surface is nearly parallel to the scanner's beam), the light may be spread over some length of the surface at varying distances from the scanner. This may result in a relatively long duration of time between the first and the last instances of light returning to the sensor. There are similar circumstances when the light beam intersects a surface near the edge of a feature. Some of the light may be reflected by a foreground feature and the remainder reflected by a background feature. The time between the first, intermediate, and last returns may be averaged for calculation of the distance from the scanner. This may result in some data points that are appear to be 'back-spraying' from edges of foreground features to the background.

The *maximum angle* parameter, ranging between 0 and 89.9 degrees, can remove points associated with surface normals greater than the specified angle. Such measurements tend to be noisy due to the averaging of first and last returns for the distance calculation. Data like this will typically not represent the true character of the surfaces and their use should be avoided.

Careful attention is suggested, however, so as not to remove data that is necessary. For example, modeling the ground surface may require a *maximum angle* setting of approaching 90 degrees because a ground-based scanner may emit a nearly perpendicular beam of light compared to the surface normal of the ground.

For this research, several parameter settings were tested. Holding the other parameters constant, examples of varying the *maximum angle* are shown in Figure 3. The figures correspond to the features in Figure 1, above: two canal spouts (out of a capped stone-lined canal, an uncovered stone-lined canal, and a carved stone fountain pouring into a stairwell of the temple. They are also arranged per settings according to Table 1, with values of 89, 85, and 80 from top to bottom. The points are displayed in white against a black background and the images have been cropped to focus on the features of interest. More points will have a whiter appearance and fewer points will appear as dark space.

The examples show that more points are included with higher *maximum angle* values (e.g. 89 degrees), allowing for more points representing surfaces that are nearly parallel to the laser beam. If the angle is too high, there may be numerous 'back-spray' points due to interpolating foreground and background features. If the angle is too low, there will not be enough points to build a detailed surface. Based upon visual inspection, a *maximum angle* value of 85 degrees was selected since there were sufficient numbers of points to build a surface and, only perceptible with close inspection, there were not many 'back-spray' points. Just a few such points have noticeably degrading effect on a model.

Figure 3: Examples of varying the *maximum angle* import parameter (not to scale).

Import parameter: Maximum edge length

The *maximum edge length* parameter limits the length of triangle edges between original scan points. The *interpolated grid* is sampled from these triangles, so it is important to have enough coverage to sample a surface from. Like the other two import parameters, this important setting has trade-offs as well. Since the archaeological features are complex and very irregular, a fine-scale was required, especially for modeling features with a linear dimension of 10 cm.

A large *maximum edge length* can be used to connect points in regions of sparse data, filling holes in the data. This works well if the surface of interest is smooth in such under-sampled areas. However, longer triangle edges can be troublesome as they tend to incorrectly bridge over convex shapes.

A small maximum edge length produces only small triangles for a surface representation. This was helpful for reducing a 'bridging' effect over uncovered canals, their open ends, and features such as the fountains. Using a small maximum edge length also reduced a 'cobweb' effect near interior corners of floors, walls, and other structures. The effects of

varying *maximum edge length* are shown in Figure 4 with decreasing values from top to bottom. For the purposes of modeling Inca water-flow surfaces, a *maximum edge length* of 0.06 m was selected because it had the fewest (dark) empty areas. Triangles with larger edges are able to cover some gaps in the data and with other extreme large values (e.g. 0.20 m) it was apparent that more points filled in sparse areas. This parameter had a greater effect on the overall coverage than did the *maximum angle*.

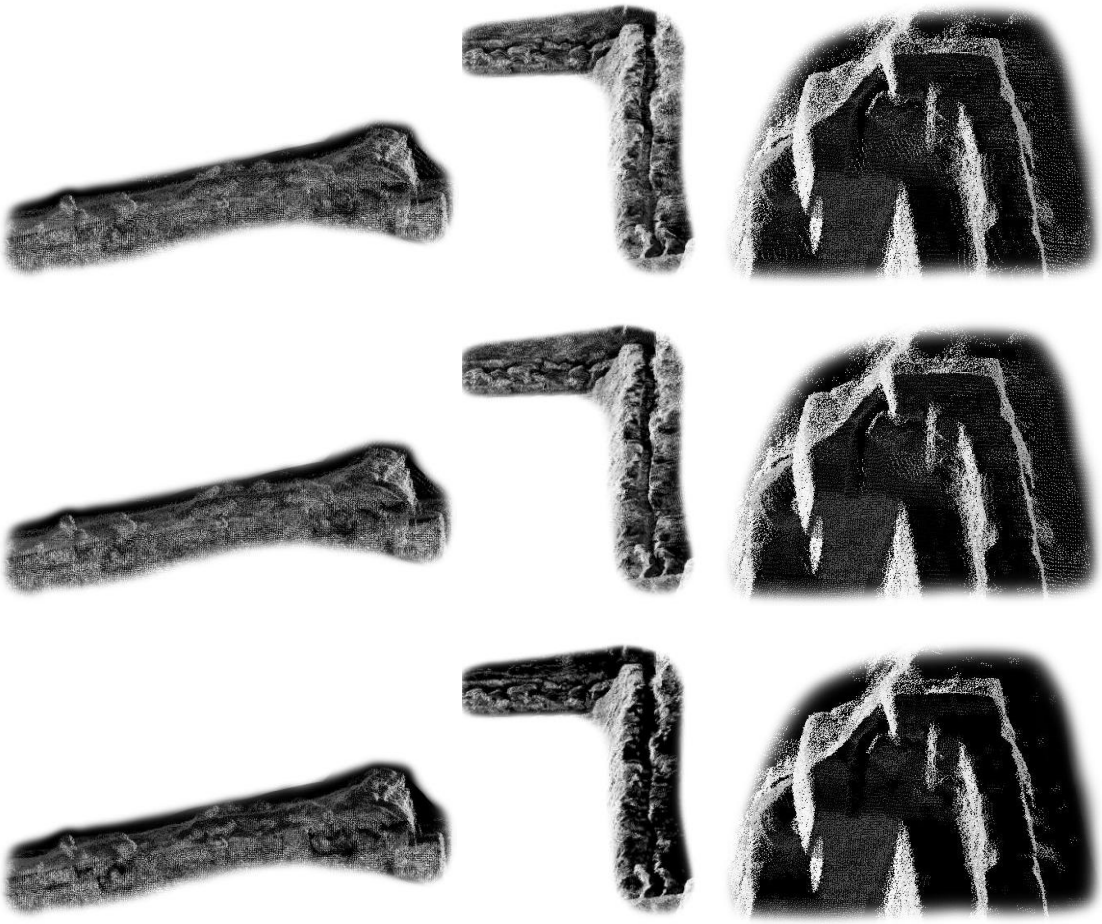

Figure 4: Examples of varying the *maximum edge length* import parameter (not to scale).

Import parameter: Interpolation step

The *interpolated grid image* is generated for aligning multiple scans and the *interpolation step* parameter specifies the distance between grid sampling points. In essence, it is the resolution of the grid. Setting smaller distances created detailed, high-resolution grids, though processing time increased and surface models sometimes appeared noisy. A larger distance created coarser, lower-resolution grids and reduced processing time. However, aligning coarse grids reduced the alignment accuracy and often produced sparse surface models.

The canal and fountain features required detailed surface models. Linear cross-sectional flow dimensions for these features ranged from approximately 10 to 34 cm. Therefore a maximum *interpolation step* of 5 cm would resolve the smallest of these features in the roughest sense. Smaller *interpolation steps* increased the representational detail as shown in Figure 5 from top to bottom. An interpolation step of 0.008 m was selected for further modeling the surface of the archaeological features for both detail and expediency.

Here the effect of increasing sampling of the interpolated grid is noticeable. Smaller interpolation steps quickly increase overall resolution and detail of the surface model. It also helps to alleviate the issue of 'bridging' across convex shapes. The main drawback is that computational time increases, as well. In some cases, the additional data sometimes produced noisy and broken up surfaces with many small holes and surface patches.

Figure 5: Examples of varying the *interpolation step* import parameter (not to scale).

Alignment of multiple LiDAR scans

After transforming the LiDAR scan points to *interpolated grid images*, the grids were used for aligning separate scans to each other. Original scans occasionally shared the same location and perspective. However, to fully represent a 3D scene, data were often

collected from different scan positions and orientations. Many perspectives were required to represent different sides of features and eliminate obscured surfaces.

Because the alignment process minimizes error between two *interpolated grids*, it is helpful to first edit the grids, keeping data for features of interest and removing unnecessary data. Stable, well-defined data was particularly beneficial. For example, buildings often have distinct walls and edges. Retaining such data provided well-defined grid forms for the alignment fitting process. On the other hand, unnecessary or unstable data representing objects that changed positions over time were deleted. Alignment accuracy would be reduced by data representing movements of people, animals, and vegetation or by site modifications, etc. Such data was removed to reduce deviations between *interpolated grids* and improve the fit for features of interest.

Two alignment types are typically performed, a *manual alignment* followed by a *best-fit alignment*. Both require interpolated grids having a partial overlap of the scanned regions. The *manual alignment* relies upon a user to select several pairs of corresponding points in two scans. With one scan position locked, the alignment-fitting process translates and rotates the second scan to a position that minimizes the deviation between the selected pairs of points. Using this pair-wise method, the scans were roughly positioned together.

The *best-fit alignment* method uses more data, from two or more overlapping *interpolated grids*. With one scan position locked, the statistical best-fit process translates and rotates the other scans by minimizing the deviations between grids. A *maximum distance* parameter limited the search neighborhood around the interpolated grid points.

Though a pair-wise *best-fit alignment* is usually produces better results than a *manual alignment*, the *best-fit* process requires the scans to be closely aligned at the start. The statistical process can not differentiate features in the data and may produce extremely erroneous results if it is not supervised by an analyst. Screen captured examples of the *manual* and *best-fit alignment* processes are shown in Figure 6.

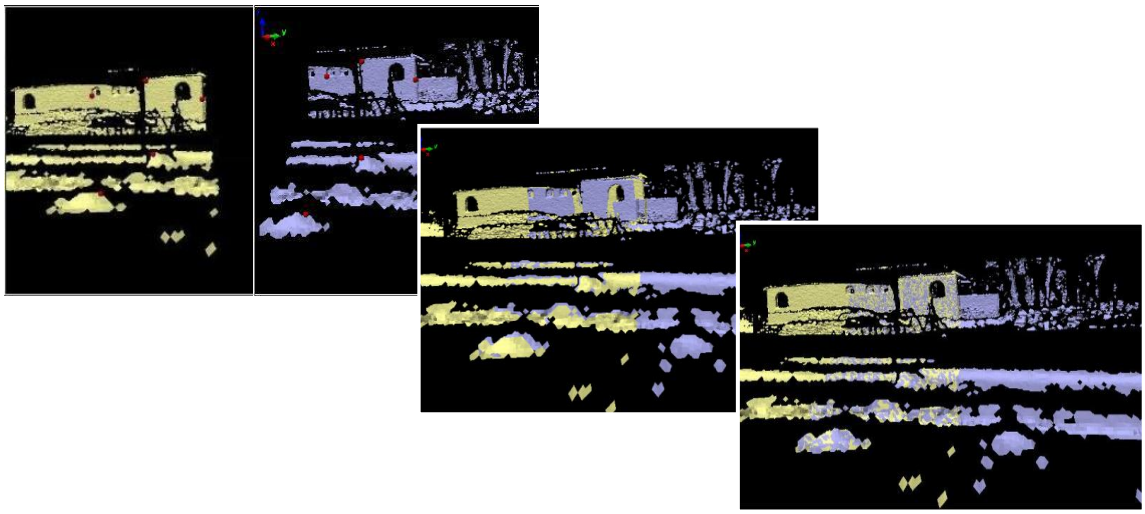

Figure 6: Examples of the *manual* and *best-fit alignment*.
Manual selection of point pairs (top), *manual alignment* results (middle),
and statistical *best-fit alignment* results (bottom).

Once the pair-wise process fit the scans tightly together, the *best-fit alignment* was used once again with just one scan locked out of the entire set. This allowed all the other scans to move freely, adjusting to the best-fit using all scans together. With visual inspection of the scan locations and the residual histograms of the scan pairs, this final all-at-once *best-fit alignment* step seemed to improve the overall results.

Orientation to horizontal and vertical control monuments

For future water-flow analysis, horizontal and vertical orientation was critical. Though the LiDAR scans were accurately aligned to each other, it was necessary to orient the data to a set of three conventional survey control monuments. Three point locations in the LiDAR data were paired with the benchmark coordinates and an *auto-matching* error minimization procedure translated and rotated the LiDAR data to the control points. The root mean squared error in the x-, y-, and z-axis was 31 mm, 28 mm, and 1 mm, respectively. Since there was so little error in the z-axis the results were acceptable.

Overlap reduction of redundant data

Many scans from different perspectives were required to create a nearly continuous 3D surface model. Though this reduced the amount of obscured surfaces, it also increased the amount of redundancy in highly visible areas. Many overlapping regions that were beneficial for alignment tended to reduce efficiency of generating a polygonal model. In order to thin the data in regions with redundant data, an *overlap reduction* process was performed. Though it is not a focus here, *overlap reduction* parameters were tested and the following values were selected: the *maximum distance* was 0.1 m, the *minimum number of layers* was 10, and the *maximum number of images* was 5. In performing this operation, the number of *interpolated grid* data was reduced by 33%.

Polygonal model generation

The final step of modeling the archaeological site surfaces created a 3D *polygonal model* from the LiDAR data. Created with the Polyworks IMMerge module, the *polygonal model* is comprised of point vertices and triangles. This type of model is a digital terrain model (DTM) that is differentiated from a digital elevation model (DEM) in that it may include more than one (z-axis) surface elevation for any (x-, y- axis) pair of horizontal coordinates. The exterior visible surfaces that are sampled may have any orientation. For example, approximately vertical sides and the undersides of overhangs can both be modeled with a DTM. In addition to the top surfaces associated with DEMs, terrestrial LiDAR can be used to generate a DTM representing surfaces of any orientation.

Polyworks has several settings for the surface generation process. Not covered here are four settings for managing the processing load, five settings for smoothing and reducing data, and a standard deviation value for specifying the amount of random variability of the scanner's measurements. Two particular parameters having a major effect on the output are the *interpolation step* and the *maximum distance*, described in the next two sections about merging scans into *polygonal models*. The previously selected import parameters (*maximum angle* 85°, *maximum edge length* 0.06 m, and *interpolation step* 0.008 m) were used in conjunction with the merging parameter settings listed in Table 3.

Table 3: Merging parameter settings for examples.

Maximum Distance	*Surface Sampling Step*
0.005	0.01
0.01	0.01
0.02	0.01
0.02	**0.01**
0.02	**0.005**
0.02	**0.002**

Merging parameter: Maximum distance

The *maximum distance* setting in the merging process is similar to the import and alignment parameters of the same name only in that it is a neighborhood search distance. Here, it specifies a threshold for determining whether portions of nearby scans are considered overlapping. If they are closer than the maximum distance they are considered overlapping and will be merged together. The result will be a single surface positioned in between them.

Immediately apparent in the surface generation step was the trade-off between having sharp edges and having a discontinuous model. In order to maintain detail and create accurate surfaces at the data locations, small, local parameters were required. If larger distances were used to connect extensive regions and fill in gaps, then the model became smoother. In the interest of maintaining detail for the water features, many of the resulting models were patchy. Ultimately, it may be better to avoid smoothing the model and keep the resulting surface as near to the data as possible.

Fine-scale merging parameters were tested in the aim of maintaining detail. At any scale, when the *maximum distance* increases, more surfaces are considered overlapping and will be merged into a single, intermediate surface. The extreme patchiness of the irregular and complex surface was slightly reduced with the largest of the parameters tested here. Trying to find a balance between detail and surface continuity, 0.02 m was selected as a fine-scale *maximum distance* parameter in the following steps. Examples of merged *polygonal models* are shown in Figure 7 having increasing *maximum distance* parameters from top to bottom.

Figure 7: Examples of varying the *maximum distance* merging parameter (not to scale).

Merging parameter: Interpolation step

The *interpolation step* in the merging process is similar to the *surface sampling step* import parameter. Here, the *interpolation step* specifies the sampling distance used for creating the *polygonal model*. Smaller values increase resolution as well as processing time. Though small step sizes helped to create a detailed surface model, another effect was increased noise. As interpolation steps decreased, smooth and potentially inaccurate models began to have slightly bumpy surfaces, but crisp edges and smaller gaps.

Examples of varying the *interpolation step* are shown in Figure 8, with decreasing step sizes from top to bottom. An *interpolation step* of 0.002 m represents an irregular and complex surface model with detail. It appears somewhat grainy though and some may find the slightly smoother model from an interpolation step of 0.005 m more aesthetically pleasing. Figure 9 shows the final model selections, improved by post-processing with automatic and manual hole-filling processes. Since the surface had not previously been excessively smoothed and the holes were relatively small, it can be expected that most of the model follows the original measurements.

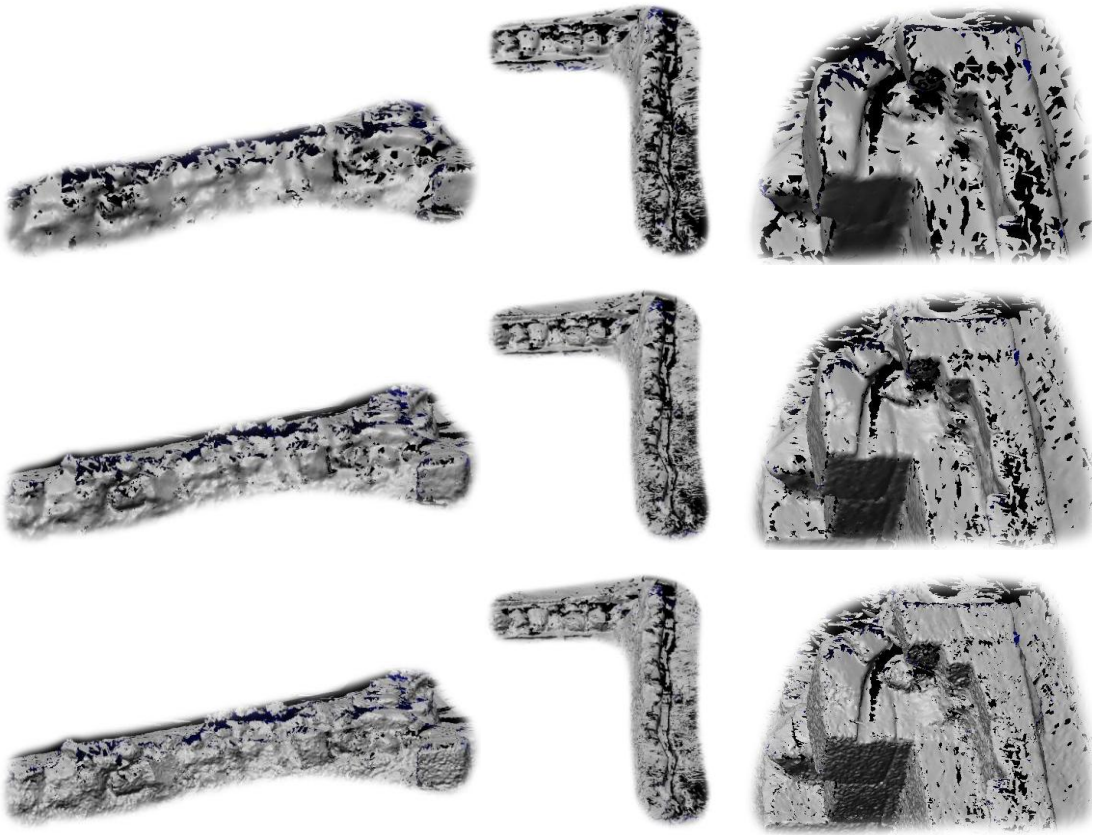

Figure 8: Examples of varying the *surface sampling step* merging parameter (not to scale).

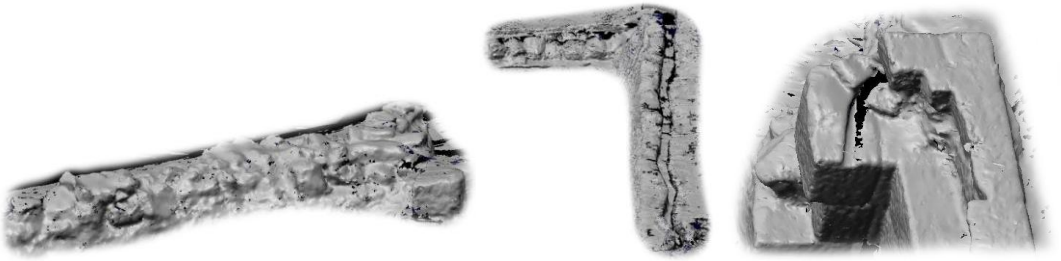

Figure 9: Examples of final models after slight post-processing (not to scale).

Results

To represent the water-flow surfaces at an archaeological site, a core requirement is the accurate location and detailed characteristics of the features. Mapping the water features at Inca-Caranqui provided an opportunity to evaluate the compromises between several surface modeling parameters. There are noticeable differences in the results depending upon import and merging parameters. For instance, the polygonal models all had some degree of patchiness which could be improved with further work.

Overall, the resulting polygonal models provide more information than conventional survey points. By using high resolution terrestrial LiDAR surface data, it was possible to not only ascertain the elevation of features, but also construct a detailed 3D model of the Inca Caranqui archaeological site in Ecuador. Complex and irregular features following

meandering paths were better represented in a three-dimensional virtual environment for detailed analysis. The extensive coverage of high resolution 3D data will help to obtain many measurements that may not have been manually taken while at the site. Being able to see inside of canal openings and underneath overhangs will contribute to thoroughly evaluating the site and the potential courses of water-flow. The resulting model provides groundwork for further study of the possible function and importance of water at the site.

Acknowledgements

I gratefully acknowledge the support and cooperation of the following individuals and organizations: Dr. Tamara Bray, for her continued support and generous guidance in understanding the archaeological concerns at Inca-Caranqui; Dr. Timothy Wawrzyzniec and Jed Frechette, M.S., for their support and guidance with understanding the data and processing of terrestrial LiDAR; and the University of New Mexico LiDAR Lab, for generously providing terrestrial LiDAR equipment. I appreciate all of your contributions.

References

Bray, T. and Echeverría, J. (2009) Saving the Palace of Atahualpa: The Late Imperial Site of Inca-Caranqui, Imbabura Province, Northern Highland Ecuador. http://www.doaks.org/research/pre-columbian/pre-columbian-project-grant-reports-1/doaks-pco-project-grant-report-2008 Last visited 8/15/2012.

Bray, T. and J. Echeverria (2010) *Informe Anual para el Proyecto " La Arquitectura de Poder: Investigaciones al sitio Imperial Tardio de Inca-Caranqui, Ibarra, Ecuador, Fase 2 (2009)."* Manuscript on file at the National Institute of Cultural Patrimony, Quito, Ecuador.

Bray, T. (2012) Water, Ritual and Power in the Inca Empire. *Latin American Antiquity*.

InnovMetric, Polyworks, version 11. (2012) http://www.innovmetric.com/polyworks/3D-scanners/home.aspx?lang=en Last visited 8/15/2012.

Lansing, S. (2006) *Perfect Order: Recognizing Complexity in Bali*. Princeton: Princeton University Press.

Sherbondy, J. (1987) Organización hidráulica y poder en el Cuzco de los Incas. *Revista Española de Antropología Americana*. 17, pp. 117-153.

Strang, V. (2004) *The Meaning of Water*. New York: Routledge.

Wright, K. and Valencia, A. (2000) *Machu Picchu: A Civil Engineering Marvel*. Reston: ASCE Press.

Wright, K. (2006) *Tipon: Water Engineering Masterpiece of the Inca Empire*. Reston: ASCE Press.

Boleslo E. Romero, Department of Geography, University of California, Santa Barbara, CA 93106. Email <bo_romero@geog.ucsb.edu>